JACS
JOURNAL OF THE AMERICAN CHEMICAL SOCIETY
pubs.acs.org/JACS
Article

^{17}O Labeling Reveals Paired Active Sites in Zeolite Catalysts

Kuizhi Chen,* Anya Zornes, Vy Nguyen, Bin Wang, Zhehong Gan, Steven P. Crossley, and Jeffery L. White*

Cite This: J. Am. Chem. Soc. 2022, 144, 16916−16929
Read Online
ACCESS | Metrics & More | Article Recommendations | Supporting Information

ABSTRACT: Current needs for extending zeolite catalysts beyond traditional gas-phase hydrocarbon chemistry demand detailed characterization of active site structures, distributions, and hydrothermal impacts. A broad suite of homonuclear and heteronuclear NMR correlation experiments on dehydrated H-ZSM-5 catalysts with isotopically enriched ^{17}O frameworks reveals that at least two types of paired active sites exist, the amount of which depends on the population of fully framework-coordinated tetrahedral Al (Al(IV)-1) and partially framework-coordinated tetrahedral Al (Al(IV)-2) sites, both of which can be denoted as $(SiO)_{4-n}$−$Al(OH)_n$. The relative amounts of Al(IV)-1 and Al(IV)-2 sites, and subsequent pairing, cannot be inferred from the catalyst Si/Al ratio, but depend on synthetic and postsynthetic modifications. Correlation experiments demonstrate that, on average, acidic hydroxyl groups from Al(IV)-1/Al(IV)-2 pairs are closer to one another than those from Al(IV)-1/Al(IV)-1 pairs, as supported by computational DFT calculations. Through-bond and through-space polarization transfer experiments exploiting ^{17}O nuclei reveal a number of different acidic hydroxyl groups in varying Si/Al catalysts, the relative amounts of which change following postsynthetic modifications. Using room-temperature isotopic exchange methods, it was determined that ^{17}O was homogeneously incorporated into the zeolite framework, while ^{17}O → ^{27}Al polarization transfer experiments demonstrated that ^{17}O incorporation does not occur for extra-framework Al_nO_m species. Data from samples exposed to controlled hydrolysis indicates that nearest neighbor Al pairs in the framework are more susceptible to hydrolytic attack. The data reported here suggest that Al(IV)-1/Al(IV)-2 paired sites are synergistic sites leading to increased reactivity in both low- and high-temperature reactions. No evidence was found for paired framework/nonframework sites.

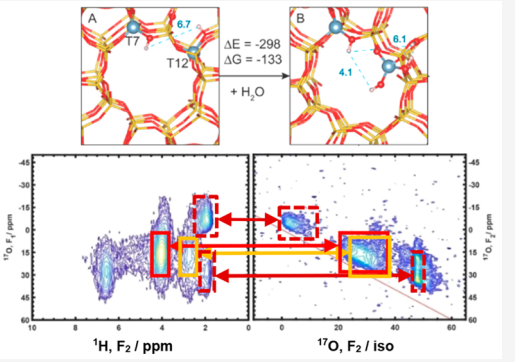

INTRODUCTION

Uncertainties surrounding long-standing questions about the nature of the active site in zeolite catalysts have been magnified by the recent discoveries of active site structure distributions, and the growing recognition that proximate Al sites in the framework may act as synergistic sites.[1−10] Whether the sites responsible for C−C, C−H, C−O, and O−H bond activation exist as isolated or paired Brönsted acid sites, whose generation through synthesis or loss from hydrothermal treatments is irreversible, or as paired and dynamic sites with mixed but temporal Brönsted and Lewis character are questions that have been pushed to the forefront of heterogeneous catalysis research by the growing need to adapt zeolites as catalysts in demanding processes other than high-temperature gas-phase hydrocarbon conversions.[11−15] Increasing environmental pressures require that catalysts convert moisture- and oxygen-rich feedstocks, including agricultural, municipal, and technological waste streams, and their diverse structural variety and environmentally benign characteristics make zeolites attractive choices for these new areas.[16−20] Even in traditional gas-phase hydrocarbon conversion processes like cracking and reforming, growing environmental pressures require increased selectivity to target molecules. In order for zeolites to be successfully extended beyond the realm of gas-phase Brönsted acid catalysis involving pure hydrocarbon feeds, characterization of active site structures as it relates to isolated vs paired framework and nonframework Al sitings, and their dynamics in the presence of other oxygen-rich and water-rich molecules, must be addressed.

One of the most intriguing and pursued topics in current zeolite science involves the synthesis, characterization, and impact of proximate Al atoms in the zeolite framework, typically termed paired sites, and concomitant questions regarding acidic hydroxyl group types.[21−25] Several recent reports highlight the difficulty in experimentally assessing framework Al pairing in MFI zeolites, some of which are commercially important in cracking, isomerization, and methanol-to-hydrocarbon conversions. Specifically, Gounder and co-workers have shown that using mixed structure-

Received: May 24, 2022
Published: August 31, 2022

https://doi.org/10.1021/jacs.2c05332
J. Am. Chem. Soc. 2022, 144, 16916−16929

directing agents during synthesis can impart some degree of control on Al siting in the framework among the 12 crystallographically inequivalent tetrahedral sites, as well as the number of paired Al sites.[26,27] Indeed, their synthetic approach has been successfully implemented for both CHA and MFI zeolites to some degree, with mixtures of charged and uncharged template molecules leading to more isolated Brönsted sites in some cases.[26−30] Other studies on zeolites with high framework Al density, e.g. HY, have shown that the expected paired Brönsted sites convert to Brönsted−Lewis pairs following hydrothermal treatments and framework dealumination.[31] Others have shown that varying the Si and Al sources, e.g. colloidal silica vs TEOS (tetraethylorthosilicate) and a variety of Al salts, can lead to different amounts of Al in different framework positions relative to the location of the SDAs.[22,23] Dusselier and others have used "seeding"-based methods and temporal changes in the synthesis compositions to effect interzeolite conversions, and final Al siting based on controlling Al mobility in the synthesis gels.[3,4] Zoned and core−shell Al distributions have been discussed by Rimer and co-workers, revealing key aspects of specific siting in framework positions versus spatial gradients in Al density throughout the crystallites.[1]

Cu^{2+} or Co^{2+} titrations are often used to identify proximate acid sites in zeolites, with detection via UV−vis or IR spectroscopies.[26−30] In addition, recent work shows that ^{1}H solid-state NMR standard-addition methods can be used to directly quantify divalent cation titration and the fraction of proximate acid sites in MFI catalysts, with some advantages as the method avoids potential false-positive spectrophotometric signals from physisorbed cations.[9,32] For example, in a commercial Si/Al = 15, approximately 35% of all acid sites were paired, whereas only 10% were found to be proximate in a different commercial catalyst with Si/Al = 40, in agreement with other reports on MFI catalysts prepared with similar structure-directing agents.[26,32] What is clear is that the number of paired acid sites depends on the synthesis procedures used to make the catalysts as well as on postsynthetic history. While many elegant experimental and computational methods have been recently reported to support the presence of paired acid sites, questions remain about the structural and temporal details of paired acid sites. For example, are all paired framework active sites composed of the standard bridging hydroxyl groups, or can one or more of the paired sites have a modified or "defective" structure? Can characterization methods unequivocally separate paired framework sites from a framework/nonframework pair, e.g. as is often termed a synergistic Brönsted/Lewis pair? Are all of the possible hydroxyl groups resulting from 12 crystallographically inequivalent Al sites and 26 different framework O atom sites, e.g. in an MFI catalyst, structurally equivalent?

In this contribution, ^{17}O-labeling of MFI catalyst frameworks are used to reveal paired-acid site structures. A quadrupolar nucleus, ^{17}O, does not lend itself to routine magic-angle spinning (MAS) NMR experiments on zeolite catalysts as originally reported by Oldfield and co-workers, due to quadrupolar coupling constants of several megahertz (MHz) depending upon the hydration level of the catalyst.[33]^{17}O NMR analyses of zeolite catalysts have been previously used by the Gray group to characterize acid sites in several zeolite catalysts, revealing detailed information regarding the quadrupolar parameters for ^{17}O in faujasite, mordenite, and MFI catalysts, as well as some O−H bond distances.[34−37] Earlier ^{17}O NMR studies demonstrated that ^{17}O quadrupolar and chemical shift parameters for zeolitic oxygen were influenced by cations and other nonframework species in naturally occurring zeolites.[38,39] Recently, the combined use of DNP (dynamic nuclear polarization) with ^{17}O NMR detection at natural abundance provided accurate O−H bond distances and a measure of bond lability in amorphous silica−aluminas.[40] Here, the combined use of heteronuclear and homonuclear correlation experiments involving ^{1}H, ^{27}Al, and ^{17}O on MFI catalysts with Si/Al ranging from 11.5 to 40 shows that at least two types of paired active sites exist, the amount of which depends on the population of fully framework-coordinated tetrahedral Al (Al(IV)-1) and partially framework-coordinated tetrahedral Al (Al(IV)-2) framework sites. Both the Al(IV)-1 and Al(IV)-2 sites obey the empirical formula $(SiO)_{4-n}-Al(OH)_n$. Partially coordinated framework Al, i.e., Al(IV)-2, was previously proposed based on computational work[41] and has recently been verified in MFI catalysts by experiment.[10,42] The relative amounts of Al(IV)-1 and Al(IV)-2 sites, and subsequent pairing, cannot be inferred from the catalyst Si/Al ratio, but is a function of synthetic and postsynthetic modifications. Well-known postsynthetic treatments involve exposing the catalyst to wet-air streams at ca. 300−600 °C, known as "steaming", cation exchanges, or chemical reagents like $SiCl_4$ or AHFS (ammonium hexafluorosilicate), all of which can impact the number and type of Al atoms in the framework or in proximity to the active sites of the framework. Comparison of newly resolved structural details on Al(IV)-1/Al(IV)-2 pairs with previous literature reports on both room-temperature and high-temperature reactions suggests that such pairs might confer additional reactivity compared to catalysts containing only traditional Al(IV)-1/Al(IV)-1 pairs.[10,42,43] The introduction of ^{17}O sites affords unprecedented resolution of a number of hydroxyl groups through $^{17}O-^{1}H$ heteronuclear correlation experiments, revealing some new sites, allowing confirmation of previously proposed proton site assignments, and extending them to include paired sites. Further, detailed correlation experiments coupled with DFT calculations show that Al−Al distances for Al(IV)-1/Al(IV)-2 pairs are less than those from Al(IV)-1/Al(IV)-1 pairs. ^{17}O incorporation does not occur for nonframework Al_nO_m species, thereby diminishing the possibility that a reversible framework/nonframework pathway exists for Al_nO_m exposed to room temperature water.

EXPERIMENTAL SECTION

Catalyst Preparation. Zeolite ZSM-5 samples with different aluminum contents (Si/Al = 40 CBV 8014, Si/Al = 15 CBV 3024E, and Si/Al = 11.5 CBV 2314) were obtained from Zeolyst in the ammonium-exchanged form. In general, dehydrated HZSM-5 zeolite samples were prepared from the ammonium form in a glass reactor body via a stepwise vacuum procedure to a final temperature of 450 °C, under 2×10^{-5} Torr using an Edwards EO4K diffusion pump.

Steaming and AHFS Treatment. AHFS (ammonium hexafluorosilicate) washed catalysts were obtained by washing as-received NH_4-ZSM-5 with AHFS, with detailed procedures described previously.[44] The "mild-steamed" catalyst was prepared by heating at 500 °C for 72 h in a home-built flow reactor, under a 12 mL/min dry N_2 flow with 17 Torr water vapor (saturated vapor pressure at ambient lab temperature). Catalysts exposed to "severe steaming" conditions followed the same procedure, but at 600 °C. The steamed samples were dehydrated following the same procedure for dehydrating as-received samples as described above.

^{17}O Enrichment. The proton form of zeolite samples, i.e., as-received, AHFS treated, or steamed at appropriate Si/Al ratios, were each well mixed with $H_2{}^{17}O$ (liquid, 90% enriched) at 70 mg catalyst/

https://doi.org/10.1021/jacs.2c05332
J. Am. Chem. Soc. 2022, 144, 16916−16929

70 μL $H_2{}^{17}O$, to form a slurry for ^{17}O enrichment, following the method proposed by Ashbrook et al. recently.[45,46] To clarify, isotopic enrichment occurred after any postsynthetic treatments. Each mixture was kept for 14 days to ensure efficient ^{17}O exchange and then used as hydrated zeolites for NMR experiments. To dehydrate, the sample was then carefully transferred into a 4 mm MAS NMR rotor and dehydrated under vacuum, at 450 °C for 5 h. The ^1H MAS NMR spectrum was always acquired to verify a complete removal of the water peak at ca. 6−7 ppm. For NMR spectrometers that were only equipped with 3.2 mm probes, the dehydrated catalyst was carefully transferred from 4 mm to 3.2 mm rotors in a glovebox, assured by the ^1H MAS NMR spectrum to rule out water contamination.

NMR Hardware and Sample Packing. NMR experiments were recorded on a variety of instruments at 9.4, 14.1, 18.8, and 19.6 T (^1H Larmor frequencies at 400, 600, 800, and 830 MHz), with Bruker Avance II, III or NEO consoles. On the 9.4 T instrument, samples were packed in 4 mm zirconia rotors with grooved Teflon spacers for further sealing, as described previously.[9] On the 14.1, 18.8, and 19.6 T instruments at NHMFL, samples were packed in Al-free 3.2 mm zirconia Pencil rotors purchased from Revolution NMR. For zirconia Pencil rotors, sulfur powders were copacked to provide an additional seal to the sample, as demonstrated previously.[42] The magic-angle spinning rates are indicated in the text accordingly for the specific experiments.

1D ^{17}O NMR. 1D ^{17}O spectra were acquired by spin−echo sequences, with a central transition (CT) selective 90°- and 180°-pulse of 9 and 18 μs, respectively, and recycle delay of 0.2 s.

2D $^1H-^{17}O$ Correlation. For dipolar coupling based experiments, proton-detected $^1H\{^{17}O\}$ D-HMQC (dipolar heteronuclear multiple quantum coherence) was employed, as it provides increased sensitivity and stability.[47,48] $SR4_1^2$ recoupling sequences[47,48] were applied at various mixing times as stated in the text accordingly, where 80 rotor-synchronized t_1 increments were normally applied. For J-coupling based experiments, excitation was also applied on the ^1H channel, with 80 rotor-synchronized t_1 increments. As a consequence of proton detection, the recycle delay is determined by the ^1H spin−lattice relaxation constant (T_1), which is determined by trace water adsorptions, as demonstrated in our previous work.[9,42] For the samples used in this work, the recycle delay value for proton detected $^1H-^{17}O$ correlation experiments varied from 0.2 to 0.5 s per optimization. Typically 128 or 256 scans were acquired, depending on the specific spectral quality desired. Thanks to the high sensitivity of the proton detection method, a 2D HMQC spectrum can usually be acquired in 1 to 3 h.

2D MQMAS. The z-filter[49,50] MQMAS (multiple-quantum magic-angle spinning) ^{17}O sequence was employed at MAS = 16 kHz, with 100 rotor-synchronized t_1 increments, a recycle delay of 0.1 s, and 2400 scans, yielding typical experimental times of 8 h. The MQMAS data were processed with a Q-shear transformation to expand the F1 spectral width.[51]

2D $^1H-^1H$, $^{27}Al-^{27}Al$, and $^{17}O-^{17}O$. DQ-SQ (double-quantum single-quantum) experiments were used for establishing homonuclear correlations. A BABA (back-to-back) recoupling sequence was used to generate ^1H DQ coherence.[52] $BR2_2^1$ homonuclear dipolar recoupling sequences were used to generate DQ coherence for quadrupolar nuclei ^{27}Al and ^{17}O,[53] where a central-transition (CT) π pulse was placed during the t_1 evolution to reject DQ-ST (satellite transitions) coherences, and thus ensure all signals arise from CT-CT DQ coherence.[54] A WURST (wideband, uniform rate, smooth truncation) pulse was applied to ST before each transient for CT signal enhancement.[55] For $^{27}Al-^{27}Al$, the 2D DQ-SQ experiment was optimized for 60 rotor-synchronized t_1 increments with 0.02s of recycle delay, while those parameters were optimized as 30 rotor-synchronized t_1 increments and recycle delay = 0.1s for $^{17}O-^{17}O$ correlation. $^{27}Al-^{27}Al$ and $^{17}O-^{17}O$ experiments were carried out on the 19.6 T instrument at NHMFL, at MAS = 16 kHz. For $^1H-^1H$ DQ-SQ experiments, similar to the proton detected $^1H\{^{17}O\}$ D-HMQC experiments, the 2D experiment was optimized for 100 rotor-synchronized t_1 increments (td1) with 1 s recycle delay. It should be noted the optimal proton recycle delay can vary from 0.2 s to more than 1 s due to trace water effects, depending on the sample preparation and sealing condition, which has been demonstrated previously.[9,42] The proton T_1 is not critical to the overall conclusions, but can significantly affect the experimental time, e.g., from a few hour to a few days. In general, we selected samples with T_1 < 0.3 s, and typically set d1 = 1s, with optimized td1 = 100 for the 2D $^1H-^1H$ DQ-SQ experiment.

Computational Details. The periodic DFT calculations were performed using the Vienna ab initio simulation package (VASP)[56] version 5.4.1. The PBE generalized gradient approximation (GGA)[57] exchange-correlation potential was used with the projector augmented wave (PAW) method.[58,59] To account for the dispersion forces, the DFT-D2 method as implemented by Henklemen was employed.[60] All atoms were fully relaxed until the atomic net force on each atom was smaller than 0.02 eV/Å. The plane-wave kinetic cutoff energy was set to 400 eV.

The ZSM-5 zeolite was modeled using a unit cell consisting of 96 T-sites (Si or Al) and 192 oxygen atoms. The lattice constants were constructed from our previous studies as a = 20.078 Å, b = 19.894 Å, c = 13.372 Å and a = b = g = 90°. We choose Al(IV)-1/Al(IV)-1 pair at T7 and T12 at intersection, which are separated by 2 Si linking site for calculations of framework hydrolysis.[10,32,43]

Gibbs free energies were calculated based on a harmonic oscillator model at 500 °C, in which all the degrees of freedom are treated harmonically. The energy threshold for vibrational frequency calculations was set at 10^{-8} eV. The low-lying vibrations coming from the free rotations and translations were treated using the quasi-rigid rotor harmonic oscillator approximation (qRRHO) of Grimme[61] and Head-Gordon.[62] Additionally, gas-phase Gibbs free energy calculations were carried out using a system pressure of 1 atm.

RESULTS AND DISCUSSION

The extremely low natural abundance of ^{17}O (0.037%) coupled with its quadrupolar properties (I = 5/2) necessitates isotopic labeling of catalysts. Figure 1 shows single-pulse MAS

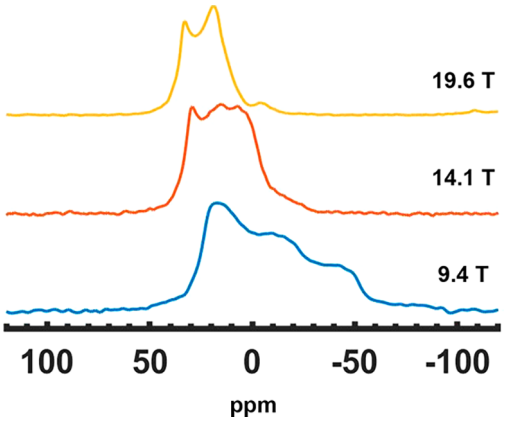

Figure 1. ^{17}O MAS NMR spectra of isotopically labeled and dehydrated HZSM-5 (Si/Al = 15) acquired at multiple field strengths as indicated.

NMR spectra for dehydrated ^{17}O-labeled zeolite HZSM-5 acquired at three different field strengths corresponding to ^1H Larmor frequencies of 400, 600, and 830 MHz. As expected from the known relative contribution of the quadrupolar interaction as a function of magnetic field strength,[10] the overall width of each spectrum decreases at higher fields. The ^{17}O labeling method results in excellent overall sensitivity, but even at 19.6 T, insufficient resolution exists to assign different oxygen chemical shifts arising from unique sites in the catalyst due to residual quadrupolar interactions, the latter of which are larger in magnitude for dry catalysts due to increased electric

https://doi.org/10.1021/jacs.2c05332
J. Am. Chem. Soc. 2022, 144, 16916−16929

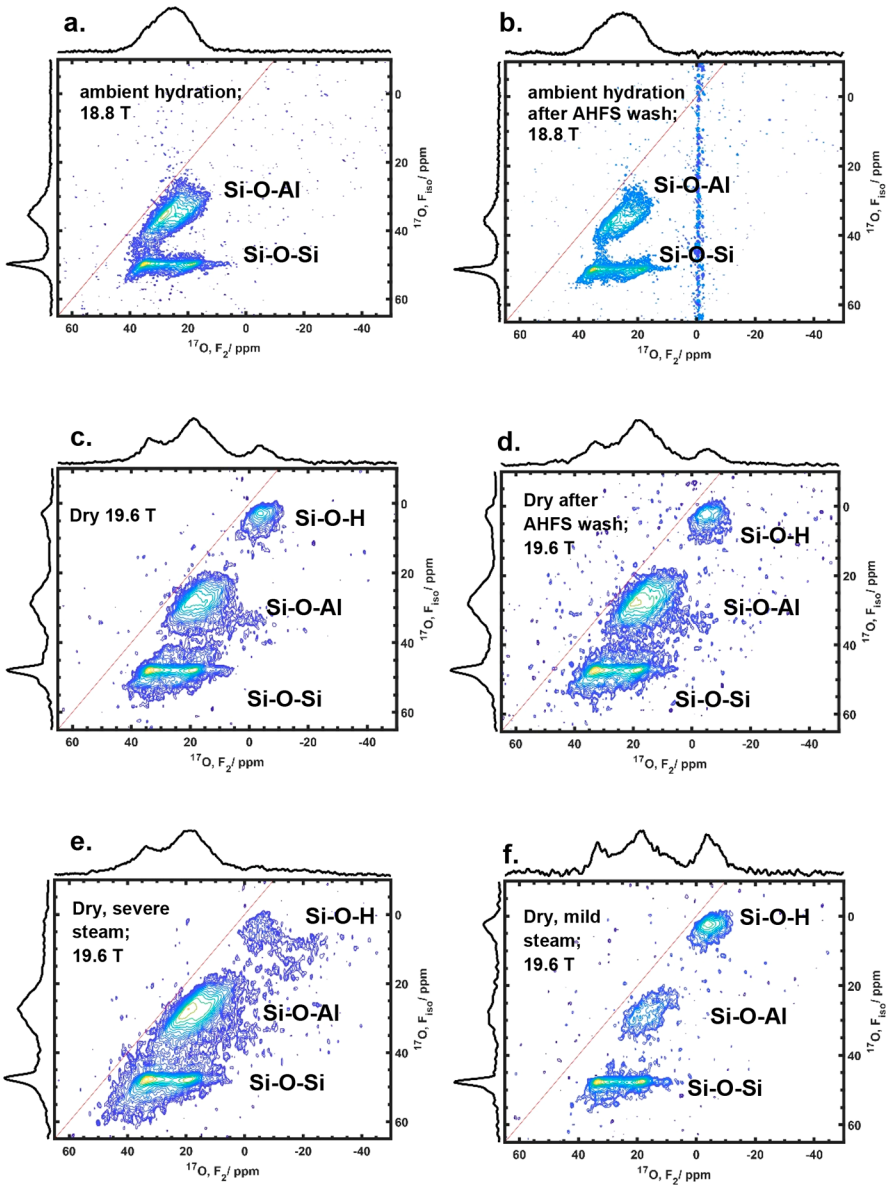

Figure 2. Overview of ^{17}O MQMAS spectra of HZSM-5 catalysts at 18.8 or 19.6 T on Si/Al = 15 (a–d), Si/Al = 11.5 (e), and Si/Al = 40 (f), with postsynthetic treatment history indicated in each figure. Spectral plots in (a) and (b) compare the effect of AHFS treatment on ambient-hydration samples; (c) and (d) compare the effect of AHFS treatment on dehydrated samples. (e) Spectra acquired on Si/Al = 11.5 after severe steaming. (f) Spectra acquired on Si/Al = 40 after mild steaming. Unless noted, samples are in their as-received H^+ form.

field gradients from the lattice strain in the absence of moisture. The 19.6 T spectrum suggests that multiple oxygen sites might exist in the dehydrated catalyst, but 2D correlation experiments that eliminate quadrupolar broadening are required to make complete assignments.

Distribution of Oxygen Atom Sites. Two-dimensional MQMAS experimental results are shown in Figure 2, providing a general overview of how various sample histories impact the 2D spectra. Figure 2c–2d show that indeed three general populations of ^{17}O sites exist, as expected based on past studies,[33−39,63] corresponding to nonacidic silanol sites (SiOH), framework oxygen atoms surrounded by only Si atoms (SiOSi), and oxygen bonded to both Si and Al atoms (SiOAl). The SiOAl signal is more complex as it may contain up to 12 T-site signals with a range of SiOAl bond angles as well as other types of SiOAl structures as will be discussed in Figure 3. Qualitative comparisons between ^{17}O chemical shifts and bond angle ranges have been reported for low-silica zeolites,[35] as well as quantitative ab initio correlations for siliceous ferrierite.[64] Interestingly, the SiOH signal does not appear in the hydrated samples (Figure 2a and 2b), presumably due to water-induced chemical exchange on an intermediate time scale that interferes with either the pulse sequence or MAS. Alternatively, the signals arising from the hydrated SiOH moieties are possibly below the noise as the triple-quantum states are not efficiently excited due to water-induced chemical exchange. A distribution of SiOAl environments is indicated by the broad signal envelope in the isotropic dimension of each 2D plot, while as expected, the projection for the SiOSi signal is relatively narrow. Also, the increased width of the summed projections in both dimensions for the dry versus hydrated samples, e.g., comparing Figure 2c/d to 2a, suggests a contribution from the quadrupolar induced shift in the former due to the increased lattice strain accompanying

https://doi.org/10.1021/jacs.2c05332
J. Am. Chem. Soc. 2022, 144, 16916−16929

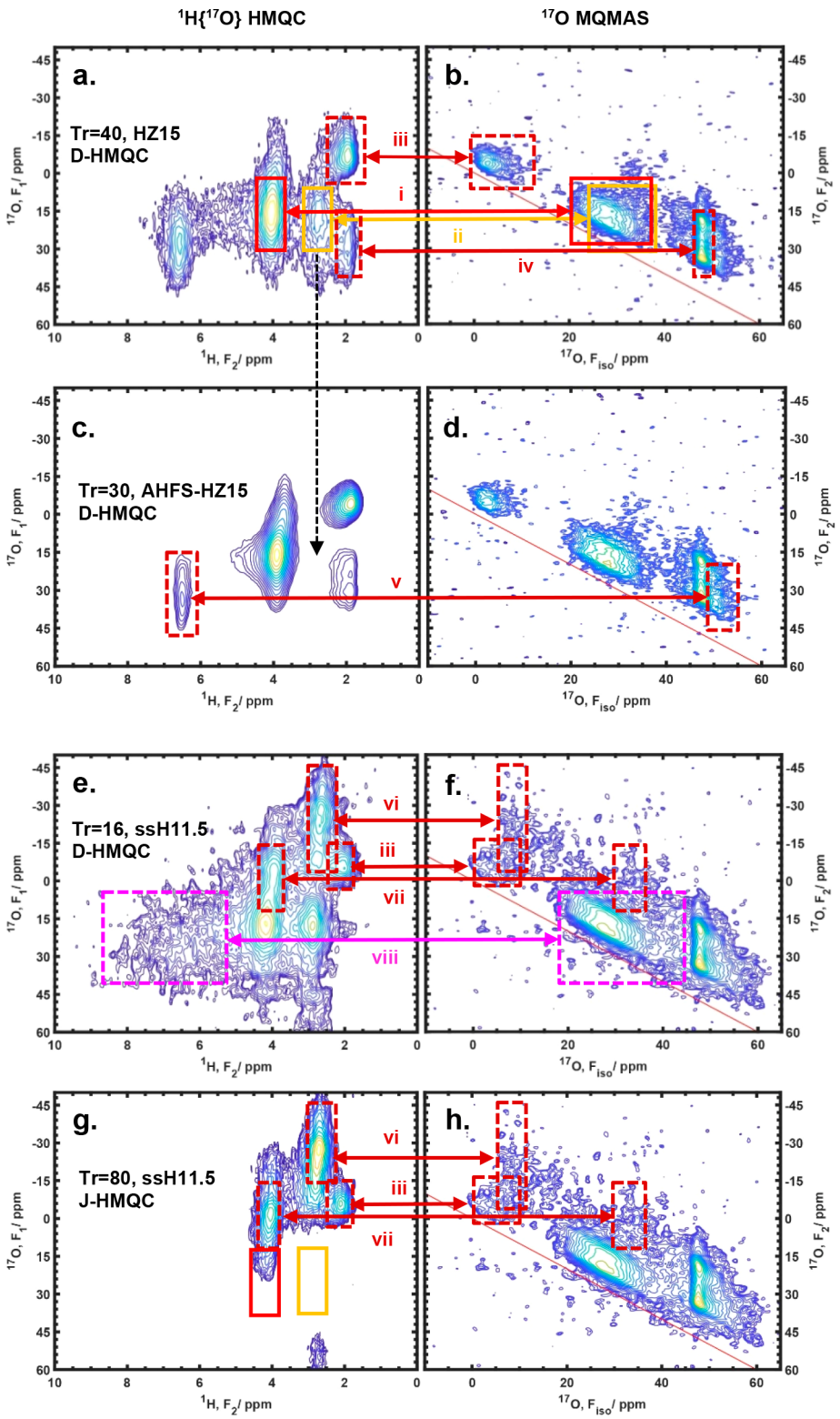

Figure 3. Correlated 2D ^{1}H{^{17}O} D-HMQC (left column) and ^{17}O MQMAS (right column) correlation spectra for dry HZSM-5 zeolites acquired at 19.6 T and with 16 kHz MAS. (a,b) Si/Al = 15; (c,d) same as (a,b) after AHFS washing; (e,f) Si/Al = 11.5 after steaming; (g,h) same as (e,f) but with J-HMQC instead of D-HMQC.

dehydration, coinciding with a range of SiOAl bond angles. Further, differences in the response of the SiOSi and SiOAl signals to hydration, as seen in Figure 2c/d vs Figure 2a/b, suggest that strong water interactions exist at the SiOAl sites and that ^{17}O data on dry samples will be critical to differentiating different framework sites. Previous investigations revealed that the Si/Al = 15 HZSM-5 catalyst used here does not have detectable amounts of nonframework Al(III) sites, but does contain a small amount of nonframework Al(VI).[42] As described in the cited reference which employed

https://doi.org/10.1021/jacs.2c05332
J. Am. Chem. Soc. 2022, 144, 16916−16929

multiple field strengths up to 35.2 T, Al(III) sites have very large electric field gradients and resulting quadrupolar interactions and can be difficult to detect in the absence of high-field data and multiple-field strength comparisons.[42] Thus, the Si^{17}OAl signals in Figure 2 must predominantly originate from oxygens at Brönsted acid sites. As will be verified by ^{27}Al−^{17}O coupling experiments shown in Figure 7 (*vide infra*), nonframework Al(VI)-coordinated oxygen does not undergo isotopic exchange using this type of isotopic labeling procedure, and thus does not contain any ^{17}O isotopes.

Stated simply, none of the signals for the nonsteamed samples in Figure 2 or 3 below can be attributed to nonframework oxygen species. For the mild- and severe-steamed 11.5 catalysts, any nonframework ^{17}O signals that might exist are from oxygen atoms that were originally in the framework. Examining Figure 2c−2f shows little variation in the number and apparent distribution of ^{17}O species, with the exception of the expected decrease in the SiOAl signal in 2f for the Si/Al = 40 sample. Analysis of slices parallel to the F_2 axis in concert with computational analysis can possibly yield additional structural details via quadrupolar parameters like the quadrupole coupling constant C_Q and asymmetry parameter η, but otherwise the amount of additional information easily accessible from Figure 2 is limited.

Correlating ^{17}O and ^{1}H Sites. A key conclusion from this work centers on the presence and structure of paired active sites in zeolites. As such, it is important to experimentally extract as much catalyst structure information as possible. The distribution of species suggested by the MQMAS data in Figure 2 can be resolved with 2D ^{1}H{^{17}O} HMQC correlation experiments. A "correlation of correlations" plot shown in Figure 3 extends new information from highly resolved ^{1}H{^{17}O} D- and J-HMQC data (left column in Figure 3) to isotropic ^{17}O shifts obtained via MQMAS (right column in Figure 3). In contrast to Figure 2 and the standard representation of MQMAS data, the MQMAS spectra in the right column are plotted differently, i.e., with the indirectly detected isotropic dimension on the *x*-axis, and the quadrupolar spectrum on the *y*-axis. Figure 3 contains a large amount of information, and a stepwise analysis of the HMQC data in the left column as well as complementary data in the Supporting Information (SI) is necessary to establish meaningful relationships to the MQMAS data in the right column, which in total will provide the most complete structural analysis of the reactive sites in the catalyst. The samples selected for representative illustration in Figure 3 represent a logical progression from an as-received, high-Al content commercial HZSM-5 catalyst (Figure 3a) to a similar catalyst following chemical washing (Figure 3c) or one subjected to hydrothermal steaming (Figure 3e). A complete series of all ^{1}H{^{17}O} HMQC data on these and other catalyst samples are provided in Figures S1−S4. ^{1}H{^{17}O}HMQC data acquired at the multiple field strengths (9.4, 14.1, 19.6 T) for the initial HZSM-5 (Si/Al = 15) and its AHFS-washed analogue, as well as several other catalysts, are shown in the SI in order to provide evidence that such experiments are not only possible but also extremely informative even at relatively modest magnetic fields. Key information from those SI data will be incorporated into the discussion below.

The dipolar recoupling time for the HMQC is the key experimental variable governing the relative signal intensities and ranges from 125 μs (2 rotor period Tr) to almost 3.7 ms (60 rotor periods) for the D-HMQC data presented throughout this work. In Figure 3, intermediate recoupling times are used that are sufficient to provide reasonable signal-to-noise for all species present, with sufficient length for dipolar couplings to evolve but short enough to avoid complications from spin−spin relaxation. For example, Figure 3a was obtained using a 40·Tr recoupling time, but comparison to a more complete series of recoupling times in Figure S1 shows that all signals are not present at the shortest dipolar mixing times, only those from the most strongly coupled O−H pairs. In the absence of significant molecular motion, the latter correspond to O−H pairs with the shortest through-space distance, which presumably will be directly bonded atoms. J-HMQC experiments transfer polarization between the O and H spins exclusively through bond, and not through space. The magnitude of the scalar or J-coupling between atoms is typically much smaller than the dipolar coupling, typically on the order of Hz vs kHz respectively, thus requiring longer recoupling times for the same relative sensitivity. In all of the HMQC data provided in the Supporting Information, one observes complete agreement between the J-HMQC plots and the D-HMQC spectra obtained at the shortest mixing times, independent of the zeolite examined and independent of the field strength. This general result, while expected, is critical to subsequent discussions on acidic vs nonacidic OH site assignment and exchange lifetimes for protons at different framework oxygen sites.

Figure 3a shows several O−H correlations for the commercial HZSM-5 Si/Al = 15 catalyst. Since the relationship between structure and activity is critical to catalyst performance, those signals corresponding to OH groups associated with Brönsted acidity are addressed first. These signals are shown in the two solid boxes and labeled **i** and **ii**, with the traditional BAS OH groups from tetrahedral framework Al (Al(IV)-1) in the red box giving rise to the ^{1}H signal at 4.2 ppm, and OH groups from the recently identified partially coordinated tetrahedral framework Al (Al(IV)-2) in the orange box with a ^{1}H signal at 2.8 ppm.[10,42] The signal in the orange box is not associated with extra-framework AlOH species, as has been thoroughly demonstrated in past works.[10,42] Within the limits of the sensitivity, signals **i** and **ii** have similar isotropic ^{17}O shifts near 28 ppm, as seen by the line connecting these signals to the boxed regions in the Figure 3b MQMAS results, confirming past results showing that each of these OH moieties are bonded to a tetrahedrally coordinated framework Al atom.

The signal labeled **iii** in Figure 3a originates from silanol OH groups on crystallite surfaces or at defect sites internal to the crystal, with an oxygen signal corresponding to the previously assigned SiOH signal region in the Figure 3b MQMAS plot. Given that Figure 3a was acquired with a relatively long dipolar recoupling period corresponding to 40 rotor periods, the additional signal **iv** at the same ^{1}H chemical shift but correlated to the SiOSi region in the MQMAS (Figure 3b) is observed due to long-range ^{17}O−^{1}H dipolar couplings that are able to evolve at longer times. Importantly, signal **iv** is not observed at the shorter recoupling times as can be seen in Figures S1 and S2. As such, signal **iv** in Figure 3a does not correspond to a separate type of hydroxyl group, but simply reflects the spatial relationship of the OH moiety (**iii**) to the rest of the siliceous catalyst matrix.

Acidic OH Groups. Chemical washing of the catalyst in Figure 3a with AHFS yields the catalyst whose HMQC results

https://doi.org/10.1021/jacs.2c05332
J. Am. Chem. Soc. 2022, 144, 16916−16929

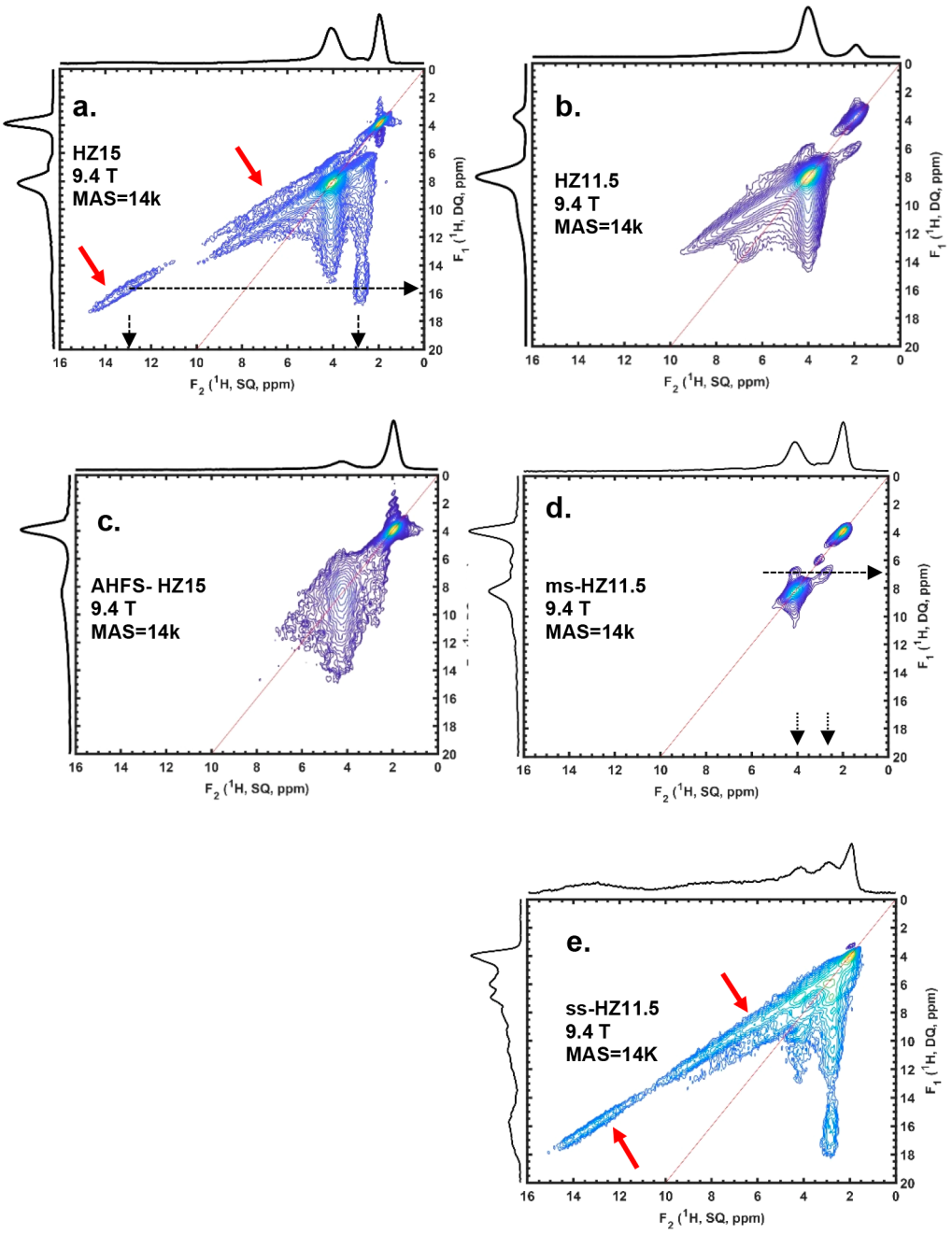

Figure 4. 2D ^{1}H DQ-SQ spectra acquired on initial and postsynthetically modified catalysts. (a) As-received HZSM-5 (15). (b) As-received HZSM-5 (11.5). (c) Same as in (a) following AHFS treatment. (d) Same as in (b) following mild steaming. (e) Same as in (b) following severe-steaming. All experiments were acquired at 9.4 T, 14 kHz MAS, with 8 rotor periods of recoupling time, i.e., 571 μs corresponding to MAS = 14 kHz.

are shown in Figure 3c, and accompanying multiple dipolar recoupling time data in Figure S2. All signals in Figure 3a persist in Figure 3c, with the important exception of the OH groups **ii** arising from hydroxyls at the framework Al(IV)-2 sites. The signal labeled **v** is due to some water contamination, i.e. ingress into the packed sample rotor, also observed in Figure 3a but not labeled there for clarity. Confirmation of this assignment is given in Figure S9, which shows that vacuum dehydration removes signal **v**. Previous work has shown that mild AHFS washing conditions remove only the Al(IV)-2 framework sites, and not the Al(IV)-1 framework atoms, and therefore signal **i** remains in Figure 3c while **ii** is completely eliminated as indicated by the black dashed arrow. Together, the results in Figure 3a, 3c, and 3d confirm that these OH groups originate from framework Si[17]OAl sites based on the Figure 3b MQMAS correlation, and not extra-framework Al structures that are historically assumed to generate signals at that ^{1}H chemical shift and for which AHFS is typically considered to remove from the catalyst. Figure 7 will further verify this result. Comparing all of the D-HMQC data for the HZSM-5 and AHFS-washed analogue in Figures S1 and S2 to their J-HMQC counterparts shows that, in all cases, signals **i** and **ii** are always absent in the J-HMQC data. For convenience, this is also shown in Figure 3g and 3h by the missing intensity in the same color red and yellow boxes for the Si/Al = 11.5 catalyst, and is true for all HZSM-5 catalysts examined to date.

https://doi.org/10.1021/jacs.2c05332
J. Am. Chem. Soc. 2022, 144, 16916−16929

The $^{1}H\{^{17}O\}$HMQC experiments reveal that proton exchange is occurring with an exchange lifetime short enough to eliminate the O−H J-coupling at *only two* sites in the zeolite, i.e., for hydroxyls at the Al(IV)-1 BAS (**i**) and the recently discovered Al(IV)-2 framework site (**ii**). Thus, ^{17}O labeling of the framework confirms that the OH groups giving rise to signal **ii** and bound to partially coordinated framework Al(IV)-2 have exchange dynamics consistent with those characteristic of the known Brönsted acid site **i**. Reducing the Al content in the catalyst reduces the number of signals observed in the $^{1}H\{^{17}O\}$HMQC experiments, as shown by the Si/Al = 40 data in Figure S3. As compared to the 40·Tr recoupling time data for Si/Al = 15 in Figure 3a, only signals **i**, **iii**, and **iv** corresponding to Al(IV)-1 BASs and SiOH groups are detected for the 40·Tr Si/Al = 40 experiment.

Additional Framework Hydroxyl Groups. Figure 3e shows HMQC results for a commercial Si/Al = 11.5 following the severe steaming treatment outlined in the Experimental Section, and acquired using 16·Tr recoupling time. The full data set for this sample as a function of recoupling time is shown in Figure S4. For clarity, the acid site correlations **i** and **ii** in Figure 3e are not labeled, but are present at the expected 2.8 and 4.2 ppm chemical shifts in the ^{1}H dimension. Two additional OH groups labeled **vi** and **vii** are easily visible in Figure 3e and 3g, which are also the first species detected at the shortest D-HMQC recoupling times in Figure S4 and in the J-HMQC spectrum for the Si/Al = 15 catalyst in Figure S1. Species **vi** has a ^{1}H chemical shift at 2.6 ppm, and from the correlation to Figure 3f the ca. 10 ppm ^{17}O shift clearly identifies this as an SiOH group. Conversely, species **vii** with a ^{1}H chemical shift of 3.9 ppm is identified as an SiOAl moiety based on the ca. 35 ppm ^{17}O shifts in Figure 3f. A similar isotropic ^{17}O shift correlation in the MQMAS spectrum of HY has been previously reported, which corresponded to an oxygen site with a large quadrupolar moment.[35] Here, with the added clarity from the complete series of $^{1}H\{^{17}O\}$HMQC data in Figure 3 and Figures S1−S4, species **vii** is revealed as a framework SiOAl hydroxyl group that has a stronger dipolar OH coupling than the previously discussed acid sites **i** and **ii**, since it appears at the shortest recoupling times and decays at a faster rate due to spin−spin relaxation at longer recoupling times. In addition, correlation **vii** is also seen in the J-HMQC data in Figure 3g and in Figures S1−S4 for the other catalysts, but neither species **i** nor **ii** is detected. In total, the correlated $^{1}H\{^{17}O\}$D-, J-HMQC, and MQMAS results suggest that species **vii** arises from a subset of framework SiOAl hydroxyl groups whose protons are static compared to the other acidic species **i** and **ii**, and in slow exchange on both the scalar coupling (Hz) and dipolar coupling (kHz) time scales and therefore potentially less acidic than species **i** and **ii**. Also, it is intriguing to observe a field-dependence of the proton chemical shift of species **vii**, which is unusual given ^{1}H is a spin-1/2 nucleus. Figure S5 presents field-dependent HMQC data regarding species **vii**, indicating the proton dipolar coupling to ^{27}Al and/or ^{17}O spins with a large quadrupolar moment impacts the ^{1}H peak position, as discussed there.

Finally, Figure 3e highlights signal **viii** showing a wide range of ^{1}H shifts that are clearly associated with the range of framework SiOAl oxygen sites in Figure 3f. These signals are also evident in the Si/Al = 15 data, albeit partially obscured by the trace water peak in Figure 3a, but clearly evident in the 9.4 T $^{1}H\{^{17}O\}$HMQC data for Si/Al = 15 shown in Figure S6 and in 14.1 T data discussed later in Figure 4. Indeed, based on prior works involving ^{1}H solid-state NMR studies of dehydrated HZSM-5, there has been extensive debate on the origin of this broad and poorly resolved signal that routinely appears from ca. 5−9 ppm in ^{1}H spectra of zeolite catalysts, and which can now be clearly associated with oxygen atoms in SiOAl sites. Previously, species with proton chemical shifts in this range have been assigned to a variety of hydrogen-bonded BASs,[65,66] hydrogen-bonded silanols,[67] strongly adsorbed water in the framework,[68] or hydroxyls on the crystallite surfaces. Our assignment to Al(IV)-2 does not necessarily exclude previous assignments from the literature, but does show it is the predominant species in HZSM-5 catalysts. Recently, we have shown that these signals are associated with the presence of hydroxyl groups from Al(IV)-2 sites,[10,42] and similar to the loss of the 2.8 ppm peak, the 5−9 ppm ^{1}H signals are also eliminated after AHFS washing.[9] Here, the correlation of the $^{1}H\{^{17}O\}$HMQC and MQMAS results shows that these signals do not arise from hydrogen-bonded SiOH sites, but are from SiOAl hydroxyl groups in the framework. Otherwise, a correlation signal to the $Si^{17}OH$ silanol signal would be observed.

Proton Proximities. The OH groups **i**−**iii** and **vi**−**viii** described in Figure 3 are not all present in all catalysts, even if they have a similar Si/Al. As explained above, AHFS-washed Si/Al = 15 catalysts and the Si/Al = 40 catalysts do not have the acidic protons **ii**, nor does the Si/Al = 11.5 catalyst in its as-received commercial form even though species **ii** is present in Si/Al = 15. However, even very mild steaming introduces species **ii** into the 11.5 catalyst, and certainly Figure 3e showed a prominent **ii** correlation after the severe-steaming step used in this work. Again, what is labeled as "severe" steaming here is much less severe than the conditions used in commercial steaming processes. The correlated $^{1}H\{^{17}O\}$HMQC and MQMAS data in Figure 3 unambiguously identify groups **i**, **ii**, **vii**, and **viii** as OH groups associated with SiOAl sites, meaning all have the potential to act as Brönsted acid sites. $^{1}H-^{1}H$ DQ-SQ experiments can be used to establish relative proximities among the chemically similar or dissimilar OH groups, i.e., **i**, **ii**, **vii**, and **viii**. Stated simply, the appearance of peak intensity in this type of experiment means that there are proton pairs that are within 0.4−0.6 nm for the experimental conditions used here, therefore strongly dipolar coupled and leading to cross-peaks whose *y*-axis chemical shift value is the sum of the chemical shifts for the two coupled ^{1}H spins, each of which corresponds to the *x*-axis values at the individual cross-peaks. The black arrows in Figure 4a and 4d illustrate this concept, showing that in Figure 4a the hydroxyl groups giving rise to the signals at 13 ppm are coupled as a dipolar spin pair to protons at 2.8 ppm (i.e., the Al(IV)-2 hydroxyl group **ii** from Figure 3), thus producing a double-quantum correlation or "cross-peak" at 15.8 ppm on the *y*-axis. Similarly, Figure 4d shows that the 4.2 ppm (**i**) and 2.8 ppm (**ii**) acidic hydroxyl group protons are dipolar coupled, yielding a correlation at 7 ppm on the double-quantum *y*-axis. The implications of these spin-pair couplings are discussed below, with the primary emphasis here to ensure that the reader understands how to interpret the data.

Figure 4 shows representative results obtained on the Si/Al = 15 and 11.5 catalysts, demonstrating that the distribution of hydroxyl groups in the initial as-synthesized catalysts is markedly different, even though both are representative of commercial high-Al content HZSM-5 catalysts and have

https://doi.org/10.1021/jacs.2c05332
J. Am. Chem. Soc. 2022, 144, 16916−16929

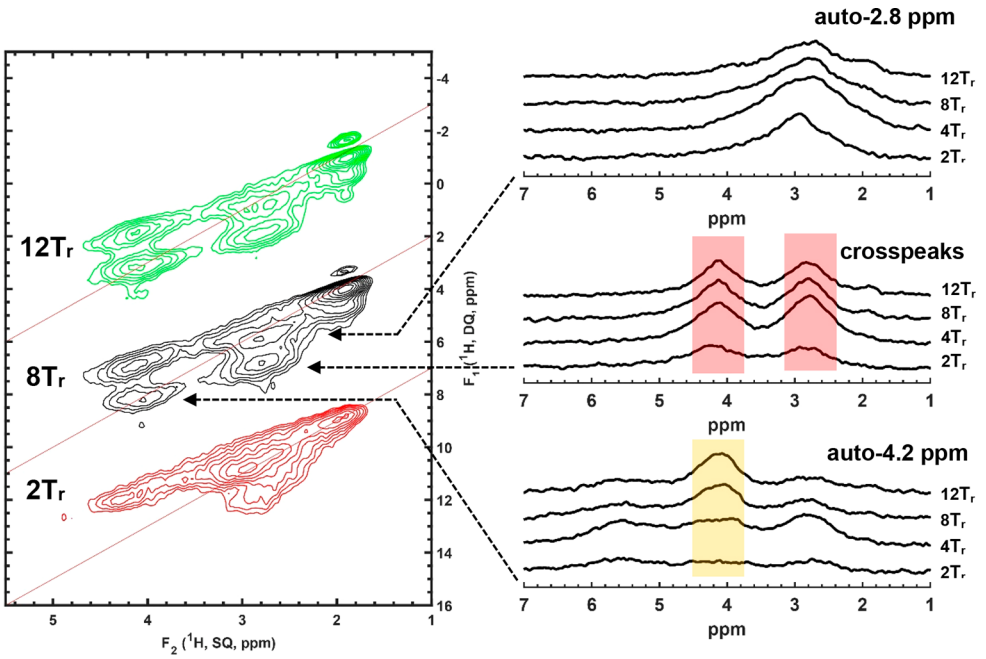

Figure 5. Fourteen kHz MAS 2D ^{1}H DQ-SQ spectra (left) with dipolar recoupling times of 2, 8, and 12 rotor periods T_r as indicated, showing the buildup trends of different proton pairs in the severe-steamed Si/Al = 11.5 catalyst. The green and red 2D spectra are plotted with vertical offsets of −5 and +5 ppm, respectively, for clarity. Projection slices (right) at F1 = 5.6 ppm (2.8 ppm autocorrelation), 6.8 ppm (2.8 ppm/4.1 ppm correlation), and 8.2 ppm (4.1 ppm autocorrelation) are arranged with increased recoupling times from bottom top as noted.

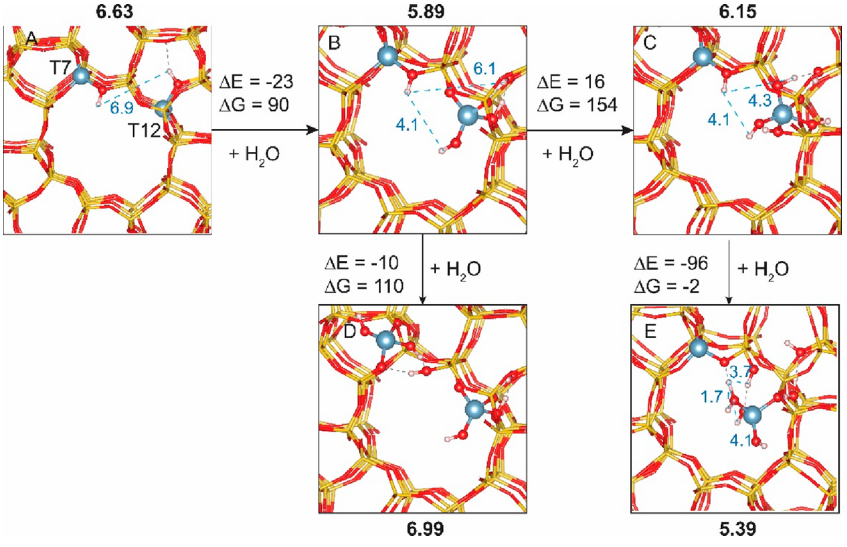

Figure 6. DFT calculations for model hydrolysis of (a) an Al(IV)-1/Al(IV)-1 pair, resulting in (b) an Al(IV)-1/Al(IV)-2 framework pair. Possible structures resulting from additional hydrolysis are shown in (c−e). Total energies and free energies are calculated with an ideal gas reference for water. The Al−Al internuclear distances (in Å) are shown in bold text above or below each structure, and H−H distances are shown in blue within each figure.

similar Si/Al. Comparing Figure 4b to 4a shows that, in agreement with the discussion above, the 11.5 catalysts do not initially have species **ii** or **viii**, the latter of which is also associated with the signals in the 10−15 ppm region of Figure 4a. The red arrows in Figure 4a denote the long "ridge" of double-quantum couplings involving the 2.8 ppm Al(IV)-2 hydroxyl group protons (**ii**) and the protons in the 5−15 ppm region of the spectrum, the length of which indicates broadening from chemical shift distribution. Such couplings are absent in the other samples shown in Figure 4b, 4c, and 4d, but are evident (red arrows) in Figure 4e which is the same 11.5 sample shown in Figure 4b after steaming treatment of the catalyst. In addition, Figure 4a, 4d, and 4e show that when the 2.8 ppm peak is present, it is coupled to 4.2 ppm BAS protons (**i**). Figure 4a and 4b demonstrate that, in both the 15 and 11.5 samples, the 4.2 ppm BAS protons are coupled to the broad 5−10 ppm signal, but not the 11−15 ppm region, thus suggesting that the chemical identity of the protons from the hydroxyl group identified as **viii** from Figure 3 and those in the 11−15 ppm region are not the same.

Observation of Paired Acid Sites. The dipolar recoupling time in the ^{1}H−^{1}H DQ/SQ experiments, as in the HMQC experiments described previously, is controlled as a function of the number of rotor periods Tr. Proton spin pairs

https://doi.org/10.1021/jacs.2c05332
J. Am. Chem. Soc. 2022, 144, 16916−16929

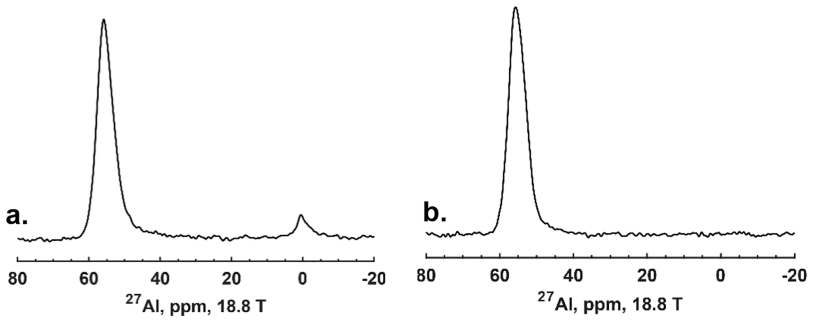

Figure 7. (a) ^{27}Al spin−echo and (b) ^{27}Al{^{17}O} J-HMQC spectra for the ^{17}O enriched Si/Al = 15 catalyst at fully hydrated condition, showing EFAl species at 0 ppm are not enriched by ^{17}O-water.

that are closest will appear at the shortest recoupling times, which was 2·Tr in this work. Figure 5 shows an expanded view of the key spectral region from ca. 1−6 ppm of ^{1}H−^{1}H DQ/SQ experiments on the Si/Al = 11.5 catalyst previously shown in Figure 4e, at mixing times ranging from 2·Tr to 12·Tr or 140−900 μs. Signals from the protons at the acid site **i** from Al(IV)-1 at 4.2 ppm and the partially coordinated framework Al(IV)-2 site protons **ii** at 2.8 ppm are visible. Extracted slices are shown in Figure 5 at the indicated recoupling times, with each of the three sets labeled corresponding to either autocorrelations between chemically similar proton pairs occur, i.e., between BAS Al(IV)-1 pairs **i/i** and Al(IV)-2 pairs **ii/ii**, versus cross-correlations between protons from proximate Al(IV)-1/Al(IV)-2 pairs **i/ii**. The variable coupling time data in Figure 5 show that the cross-correlations **i/ii** are visible at the shortest recoupling times, while the self-correlations **i/i** are not. The data in Figure 5 were collected on the steamed 11.5 catalyst, but based on identical spectral features in Figures 4a and 4e, the conclusion is the same for the as-received Si/Al = 15 catalyst. When Al(IV)-2 hydroxyl groups exist, their internuclear distance to Al(IV)-1 BAS hydroxyl groups in the catalyst is shorter than the distance between proximate Al(IV)-1 groups, and Figure 5 clearly shows that the cross-peak growth rate for **i/ii** pairs is much larger than for **i/i** pairs. Thus, the closest paired sites even in a high-Al content catalyst are not composed of the traditional BAS, but rather BAS/partially coordinated acid sites. No proximate proton **i/ii** pairs exist in the AHFS-treated catalysts. Figure S7 shows similar build-up curves for the cross-peaks appearing between the 2.8 ppm and ca. 12−15 ppm regions, again confirming that they arise from species **ii** and not from extra-framework Al species, and on a time scale similar to that of the **i/ii** pairs.

Computational Evidence for Paired Sites. In order to support the conclusions from the ^{1}H DQ-SQ internuclear distance experiments, potential transformations of an Al(IV)-1/Al(IV)-1 pair to Al(IV)-1/Al(IV)-2 pair due to partial hydrolysis were calculated using DFT, with results summarized in Figure 6. Total energies and atomic coordinate information in support of Figure 6 may be found in the SI in and immediately following Table S1. When the Al(IV)-1/Al(IV)-1 pair at T7−T12 (Figure 6A) is exposed to water vapor, one of the two framework sites will react with water. Starting with the T12 site for the reaction with water, the first hydrolysis step of T12 forms a partially coordinated acid site (Figure 6B) through an exothermic step with ΔE = −23 kJ/mol and ΔG = 90 kJ/mol. In our calculations, the T12 site is perturbed by water and displaced toward the intersection. The atomic distance of an Al(IV)-1/Al(IV)-1 pair reduces from 6.63 Å between the two framework Al to 5.98 Å for a framework Al(IV)-1/Al(IV)-2 pair, with concomitant decrease in the nearest H−H distance to 4.1 Å as well as a reduction from 6.7 to 6.1 Å for the other H−H distance. After the first Al−O bond breaking, the second water molecule may continue to attack the T12 site to break the second Al−O bond and form the configuration (Figure 6C) or react with the BAS at T7 to form a structure in Figure 6D, with free energy at about 154 and 110 kJ/mol, respectively. While not the focus of the experimental work described above, it is worth noting that, for the hydrolysis of T7, the Al site is displaced toward the sinusoidal channel, with complete hydrolysis leading to extra-framework Al that preferentially resides in the main channel intersections.[41] The Gibbs free energies for the first hydrolysis step of T7 and T12 are comparable. The difference in ΔG between the first and the second hydrolysis step of T12 is due to the structure of partially hydrolyzed Al in configuration Figure 6C. The Al site in configuration Figure 6C is five-member coordinated instead of four-member coordinated, but no Al(V) signals were detected for the samples described herein except for those severely steamed. The partially coordinated Al at T12 in the configuration (Figure 6C) can continue to react with a water molecule to form a structure (Figure 6E) with ΔG = −2 kJ/mol. After reacting with three water molecules, the Al site at T12 is only coordinated with one oxygen framework atom. This partially coordinated Al in Figure 6E further approaches the BAS at T7 and delocalizes the proton, and the Al−Al distance is reduced to 5.39 Å. We also compare the calculations with an isolated T12 site without neighboring Al sites in Figure S11. The free energy values reported here are moderately higher than literature values because gas phase water was used as the reference while physisorbed water was used previously.[41] We find that, for the first and second hydrolysis, the adjacent BAS at T7 does not affect the hydrolysis of T12; however, at the third hydrolysis step, the partially hydrolyzed Al species interact with the proton at T7 (Figure 6), which leads to a more energy favorable process when a site pair is present. In total, these calculations support the experimental observations that paired Al(IV)-1/Al(IV)-2 framework sites and their associated protons are closer than Al(IV)-1/Al(IV)-1 framework pairs.

Framework Pairs vs Framework/Nonframework Pairs. ^{17}O-labeling has the potential to clarify questions regarding synergies arising not just from paired-framework sites, as demonstrated above, but also from framework/nonframework pairs. For example, Figure 7 shows the results from important control experiments on the as-received Si/Al = 15 catalyst,

https://doi.org/10.1021/jacs.2c05332
J. Am. Chem. Soc. 2022, 144, 16916−16929

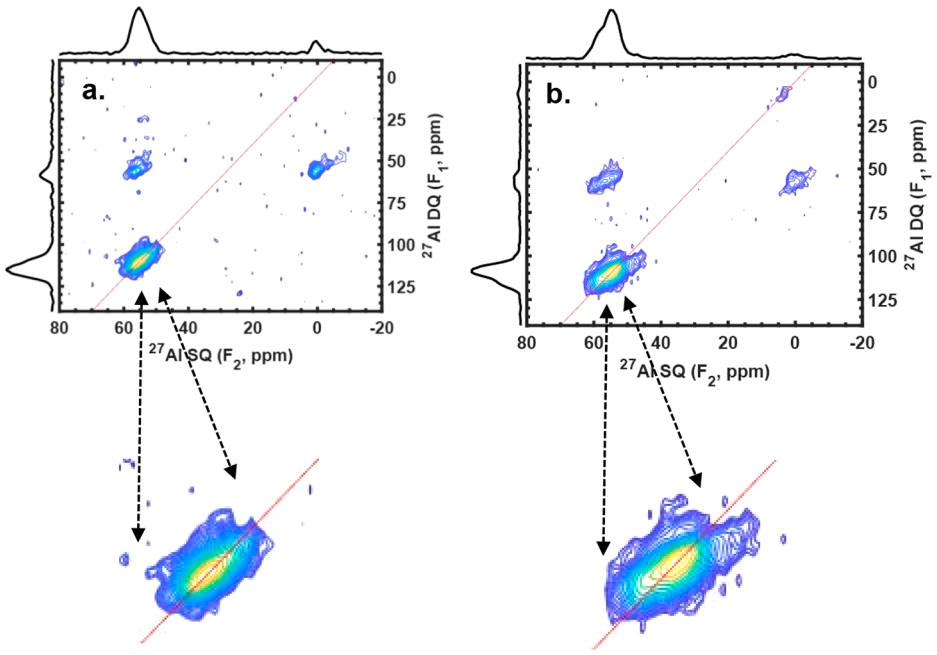

Figure 8. ^{27}Al DQ-SQ spectra of hydrated (a) ms-HZ11.5 and (b) ss-HZ11.5 acquired at 19.6 T, suggesting that dealumination preferentially occurs at paired BAS sites. Note that Al(IV)-1/Al(VI) and Al(IV)-1/Al(IV)-2 autocorrelations are both observed, but severe steaming is required to observe the Al(VI) autocorrelation signal (0 ppm in both dimensions).

comparing the quantitative ^{27}Al spin−echo spectrum (Figure 7a) to that obtained using the ^{27}Al{^{17}O} J-HMQC sequence (Figure 7b). All Al spins are detected in Figure 7a, while only those Al sites that are covalently bonded to O detected in Figure 7b. As mentioned previously in the discussion of Figure 2, some nonframework Al sites are present in the Si/Al = 15 catalyst based on the 0 ppm peak in the total Al spectrum in Figure 7a, but ^{17}O is not incorporated into those sites as shown by the absence of the 0 ppm peak in Figure 7b. The ^{17}O incorporation into the zeolite framework is efficient based on the previous data in Figures 2 and 3, which is further supported by the ^{17}O−^{17}O DQ/SQ data shown in Figure S8 of the Supporting Information. The strong cross-correlations in Figure S8 between the SiOSi and SiOAl ^{17}O spectral regions verify this claim, while the absence of a 0 ppm peak in Figure 7b shows that nonframework Al−O species do not undergo isotopic exchange. As stated in the earlier discussions of Figures 2 and 3, the data in Figure 7b are an important confirmation that all ^{17}O signals arise exclusively from oxygen sites in the zeolite framework, and importantly, including those from partially coordinated framework Al(IV)-2. In addition, these results suggest that the reversible exchange between framework tetrahedral and octahedral Al coordination does not occur when HZSM-5 is in liquid water, as has been observed in the presence of NH_3.[11]

Previous work has shown that the as-synthesized Si/Al = 11.5 catalyst has no detectable amounts of Al(IV)-2 framework sites or Al(VI) nonframework sites.[42] Mild hydrothermal treatment creates Al(IV)-2 and possibly some Al(VI) species, while severe steaming creates a significant amount of Al(VI) sites. ^{27}Al DQ-SQ results shown in Figure 8 demonstrate that Al(IV)/Al(VI) framework/nonframework pairs are detected after mild steaming (Figure 8a) as indicated by the cross-correlations between the ca. 50 and 0 ppm peaks, while severe steaming is required to generate the Al(VI) autocorrelations at 0 ppm (Figure 8b). When migration of nonframework Al species under steaming conditions is ignored, these data suggest that paired Al framework sites are the first to undergo dealumination. Given the low Al−Al DQ sensitivity in general, Al species must be in close proximity and present in relatively large quantity to yield the spectra in Figure 8. Two possibilities can lead to such results: (1) the migration of totally dislodged framework species (EFAls) to Al(IV)-1 sites, and (2) preferential hydrolysis at paired Al(IV)-1 sites. ^{1}H MAS spectra of a mild-steamed 11.5 sample show that most BAS sites remain intact after steaming, indicating the hydrothermal treatment in this case is moderate relative to typical methods. Given that such a small fraction of BAS is hydrolyzed, hydrolysis at random Al(IV)-1 sites, i.e., without preference on paired sites, will not likely yield such a strong 2.8 ppm/4.2 ppm Al(IV)-1/Al(IV)-2 correlation. One should also note that scenario 1 alone cannot yield both the correlations of Al(IV)-1/Al(IV)-2 and Al(IV)/Al(VI), but scenario 2 can, as a natural distribution of partially bonded and totally dislodged Al species will readily present when the hydrolysis favorably occurs at paired framework Al sites. At this mild steamed condition, most BASs are not yet hydrolyzed, and importantly, Figure 7 clearly shows that EFAls are not enriched by ^{17}O water, indicating that the 2.8 ppm species arises from partially bonded Al(IV)-2. As partially bonded Al framework species cannot migrate, the Figure 8 correlation indicates that Al(IV)-2 is formed at Al(IV)-1/Al(IV)-1 pairs.

Reactivity of Paired Al(IV)-1/Al(IV)-2 Sites. Prior results have shown that, upon calcination in flowing atmospheric pressure air, the HZ15 catalyst exhibits significantly higher activity per site than HZ11.5.[43] This is intriguing given the fact that extra-lattice Al(III) species are not detected even using ultrahigh fields in the starting catalysts,[42] suggesting that the paired framework sites themselves could impart increased activity similar to what has been suggested for extra lattice-framework pairs after hydrothermal treatments. Further, the fact that these proximate framework pairs are most susceptible

https://doi.org/10.1021/jacs.2c05332
J. Am. Chem. Soc. 2022, 144, 16916−16929

to hydrothermal attack, as well as the Al(IV)-2 sites being amenable to removal due to AHFS, suggests that the presence of paired framework sites could either partially hydrolyze to form active sites or under more severe conditions fully hydrolyze to create lattice/extra-lattice framework sites.

When contrasting the results reported here with those previously reported after pulsed steaming treatments, it is revealed that the HZ15 catalysts exhibit a higher final activity per site for high temperature *n*-hexane cracking.[43] This was attributed to more nonframework sites after calcination treatments in atmospheric pressure air as measured by isopropylamine temperature-programmed reduction. While it was certainly the case that after those more severe calcination treatments the proportion of protons that do not facilitate Hoffman elimination of isopropylamine is higher for the HZ11.5 zeolite than HZ15, even though more framework sites and corresponding Al(IV)-1/Al(IV)-1 pairs initially exist in the former, the relatively higher concentration of Al(IV)-1/Al(IV)-2 pairs in the initial HZ-15 zeolite is clear from the results reported here and previously.[9,42,43] These results indicate that these sites may serve as precursors to extra lattice species proximate to framework protons under more severe conditions, while potentially being responsible for high activity themselves under more mild reaction conditions and pretreatments.

CONCLUSIONS

A variety of heteronuclear and homonuclear NMR correlation experiments on ^{17}O-enriched zeolite catalysts, coupled with supporting DFT calculations, reveal that paired active sites exist in the framework. Assessment of experimental data for MFI catalysts with Si/Al ranging from 11.5 to 40 shows that at least two types of paired active sites exist, the amount of which depends on the population of fully coordinated tetrahedral Al (Al(IV)-1) and partially coordinated tetrahedral Al (Al(IV)-2) framework sites. DFT calculations show that proximate framework sites involving Al(IV-1)/Al(IV)-2 pairs are ca. 0.6−0.7 Å closer than framework Al(IV-1)/Al(IV-1) pairs, with accompanying decreases in their ^{1}H−^{1}H distances, consistent with the experimental NMR data. Heteronuclear ^{1}H−^{17}O correlation NMR experiments reveal hydroxyl group protons and oxygens arising from both Al(IV-1) and Al(IV-2) sites with unprecedented resolution. Additionally, ^{17}O → ^{27}Al polarization transfer experiments demonstrated that ^{17}O incorporation does not occur for extra-framework Al_nO_m species, and data from samples exposed to controlled hydrolysis indicate that nearest neighbor Al pairs in the framework are more susceptible to hydrolytic attack. Based on comparison to previously published data, the total data strongly suggest that these paired Al(IV-1)/Al(IV-2) sites may serve as precursors to extra-lattice species proximate to framework protons under more severe conditions, while also being responsible for high activity themselves under more mild reaction conditions and catalyst preparation.

ASSOCIATED CONTENT

Supporting Information

The Supporting Information is available free of charge at https://pubs.acs.org/doi/10.1021/jacs.2c05332.

Additional information including 2D HMQC and DQ-SQ NMR spectra, as well as atomic structure coordinate files and total energies (PDF)

AUTHOR INFORMATION

Corresponding Authors

Jeffery L. White − *School of Chemical Engineering, Oklahoma State University, Stillwater, Oklahoma 74078, United States;* orcid.org/0000-0003-4065-321X; Email: jeff.white@okstate.edu

Kuizhi Chen − *National High Magnetic Field Laboratory, Tallahassee, Florida 32310, United States;* Present Address: State Key Laboratory of Catalysis, Dalian Institute of Chemical Physics, Chinese Academy of Sciences, 457 Zhongshan Road, Dalian 116023, China. Email: kchen@dicp.ac.cn; Email: kuizhi.chen@magnet.fsu.edu

Authors

Anya Zornes − *School of Chemical Engineering, Oklahoma State University, Stillwater, Oklahoma 74078, United States*

Vy Nguyen − *School of Chemical, Materials, and Biological Engineering, University of Oklahoma, Norman, Oklahoma 73019, United States*

Bin Wang − *School of Chemical, Materials, and Biological Engineering, University of Oklahoma, Norman, Oklahoma 73019, United States;* orcid.org/0000-0001-8246-1422

Zhehong Gan − *National High Magnetic Field Laboratory, Tallahassee, Florida 32310, United States;* orcid.org/0000-0002-9855-5113

Steven P. Crossley − *School of Chemical, Materials, and Biological Engineering, University of Oklahoma, Norman, Oklahoma 73019, United States;* orcid.org/0000-0002-1017-9839

Complete contact information is available at: https://pubs.acs.org/10.1021/jacs.2c05332

Notes

The authors declare no competing financial interest.

ACKNOWLEDGMENTS

This material is based upon work supported by the National Science Foundation under Grants CHE-1764116 and CHE-1764130 and are gratefully acknowledged. Partial instrumentation support for the solid-state NMR system at Oklahoma State University was provided through the Oklahoma State University Core Facilities program. A portion of this work was performed at the National High Magnetic Field Laboratory, which is supported by the National Science Foundation Cooperative Agreement No. DMR-1644779 and the State of Florida.

REFERENCES

(1) Le, T. T.; Chawla, A.; Rimer, J. D. Impact of Acid Site Speciation and Spatial Gradients on Zeolite Catalysis. *J. Catal.* **2020**, *391*, 56−68.

(2) Bickel, E. E.; Nimlos, C. T.; Gounder, R. Developing Quantitative Synthesis-Structure-Function Relations for Framework Aluminum Arrangement Effects in Zeolite Acid Catalysis. *J. Catal.* **2021**, *399*, 75−85.

(3) Devos, J.; Robijns, S.; Van Goethem, C.; Khalil, I.; Dusselier, M. Interzeolite Conversion and the Role of Aluminum: Toward Generic Principles of Acid Site Genesis and Distributions in ZSM-5 and SSZ-13. *Chem. Mater.* **2021**, *33* (7), 2516−2531.

(4) Dědeček, J.; Sobalík, Z.; Wichterlová, B. Siting and Distribution of Framework Aluminium Atoms in Silicon-Rich Zeolites and Impact on Catalysis. *Catalysis Reviews* **2012**, *54* (2), 135−223.

(5) Knott, B. C.; Nimlos, C. T.; Robichaud, D. J.; Nimlos, M. R.; Kim, S.; Gounder, R. Consideration of the Aluminum Distribution in

Zeolites in Theoretical and Experimental Catalysis Research. *ACS Catal.* **2018**, *8* (2), 770−784.
(6) Jones, A. J.; Carr, R. T.; Zones, S. I.; Iglesia, E. Acid Strength and Solvation in Catalysis by MFI Zeolites and Effects of the Identity, Concentration and Location of Framework Heteroatoms. *J. Catal.* **2014**, *312*, 58−68.
(7) Yang, C.-T.; Janda, A.; Bell, A. T.; Lin, L.-C. Atomistic Investigations of the Effects of Si/Al Ratio and Al Distribution on the Adsorption Selectivity of n-Alkanes in Brønsted-Acid Zeolites. *J. Phys. Chem. C* **2018**, *122* (17), 9397−9410.
(8) Perea, D. E.; Arslan, I.; Liu, J.; Ristanović, Z.; Kovarik, L.; Arey, B. W.; Lercher, J. A.; Bare, S. R.; Weckhuysen, B. M. Determining the Location and Nearest Neighbours of Aluminium in Zeolites with Atom Probe Tomography. *Nat. Commun.* **2015**, *6* (1), 7589.
(9) Chen, K.; Abdolrhamani, M.; Sheets, E.; Freeman, J.; Ward, G.; White, J. L. Direct Detection of Multiple Acidic Proton Sites in Zeolite HZSM-5. *J. Am. Chem. Soc.* **2017**, *139* (51), 18698−18704.
(10) Chen, K.; Horstmeier, S.; Nguyen, V. T.; Wang, B.; Crossley, S. P.; Pham, T.; Gan, Z.; Hung, I.; White, J. L. Structure and Catalytic Characterization of a Second Framework Al(IV) Site in Zeolite Catalysts Revealed by NMR at 35.2 T. *J. Am. Chem. Soc.* **2020**, *142* (16), 7514−7523.
(11) Ravi, M.; Sushkevich, V. L.; van Bokhoven, J. A. On the Location of Lewis Acidic Aluminum in Zeolite Mordenite and the Role of Framework-Associated Aluminum in Mediating the Switch between Brønsted and Lewis acidity. *Chem. Sci.* **2021**, *12* (11), 4094−4103.
(12) Ravi, M.; Sushkevich, V. L.; van Bokhoven, J. A. Lewis Acidity Inherent to the Framework of Zeolite Mordenite. *J. Phys. Chem. C* **2019**, *123* (24), 15139−15144.
(13) Ennaert, T.; Van Aelst, J.; Dijkmans, J.; De Clercq, R.; Schutyser, W.; Dusselier, M.; Verboekend, D.; Sels, B. F. Potential and Challenges of Zeolite Chemistry in the Catalytic Conversion of Biomass. *Chem. Soc. Rev.* **2016**, *45* (3), 584−611.
(14) Li, G.; Wang, B.; Resasco, D. E. Water-Mediated Heterogeneously Catalyzed Reactions. *ACS Catal.* **2020**, *10* (2), 1294−1309.
(15) Xue, N.; Vjunov, A.; Schallmoser, S.; Fulton, J. L.; Sanchez-Sanchez, M.; Hu, J. Z.; Mei, D.; Lercher, J. A. Hydrolysis of Zeolite Framework Aluminum and its Impact on Acid Catalyzed Alkane Reactions. *J. Catal.* **2018**, *365*, 359−366.
(16) Huo, J.; Tessonnier, J.-P.; Shanks, B. H. Improving Hydrothermal Stability of Supported Metal Catalysts for Biomass Conversions: A Review. *ACS Catal.* **2021**, *11* (9), 5248−5270.
(17) Heard, C. J.; Grajciar, L.; Uhlík, F.; Shamzhy, M.; Opanasenko, M.; Čejka, J.; Nachtigall, P. Zeolite (In)Stability under Aqueous or Steaming Conditions. *Adv. Mater.* **2020**, *32* (44), 2003264.
(18) Kung, M. C.; Ye, J.; Kung, H. H. 110th Anniversary: A Perspective on Catalytic Oxidative Processes for Sustainable Water Remediation. *Ind. Eng. Chem. Res.* **2019**, *58* (37), 17325−17337.
(19) Bacariza, M. C.; Graça, I.; Lopes, J. M.; Henriques, C. Tuning Zeolite Properties towards CO2Methanation: An Overview. *ChemCatChem.* **2019**, *11* (10), 2388−2400.
(20) Zapata, P. A.; Faria, J.; Ruiz, M. P.; Jentoft, R. E.; Resasco, D. E. Hydrophobic Zeolites for Biofuel Upgrading Reactions at the Liquid−Liquid Interface in Water/Oil Emulsions. *J. Am. Chem. Soc.* **2012**, *134* (20), 8570−8578.
(21) Yang, C.-T.; Janda, A.; Bell, A. T.; Lin, L.-C. Atomistic Investigations of the Effects of Si/Al Ratio and Al Distribution on the Adsorption Selectivity of n-Alkanes in Brønsted-Acid Zeolites. *J. Phys. Chem. C* **2018**, *122* (17), 9397−9410.
(22) Li, C.; Vidal-Moya, A.; Miguel, P. J.; Dedecek, J.; Boronat, M.; Corma, A. Selective Introduction of Acid Sites in Different Confined Positions in ZSM-5 and Its Catalytic Implications. *ACS Catal.* **2018**, *8* (8), 7688−7697.
(23) Dědeček, J.; Tabor, E.; Sklenak, S. Tuning the Aluminum Distribution in Zeolites to Increase their Performance in Acid-Catalyzed Reactions. *ChemSusChem* **2019**, *12* (3), 556−576.
(24) Zhang, Y.; Zhao, R.; Sanchez-Sanchez, M.; Haller, G. L.; Hu, J.; Bermejo-Deval, R.; Liu, Y.; Lercher, J. A. Promotion of Protolytic Pentane Conversion on H-MFI Zeolite by Proximity of Extra-Framework Aluminum Oxide and Brønsted Acid Sites. *J. Catal.* **2019**, *370*, 424−433.
(25) Song, C.; Chu, Y.; Wang, M.; Shi, H.; Zhao, L.; Guo, X.; Yang, W.; Shen, J.; Xue, N.; Peng, L.; Ding, W. Cooperativity of Adjacent Brønsted Acid Sites in MFI Zeolite Channel Leads to Enhanced Polarization and Cracking of Alkanes. *J. Catal.* **2017**, *349*, 163−174.
(26) Nimlos, C. T.; Hoffman, A. J.; Hur, Y. G.; Lee, B. J.; Di Iorio, J. R.; Hibbitts, D. D.; Gounder, R. Experimental and Theoretical Assessments of Aluminum Proximity in MFI Zeolites and Its Alteration by Organic and Inorganic Structure-Directing Agents. *Chem. Mater.* **2020**, *32* (21), 9277−9298.
(27) Di Iorio, J. R.; Nimlos, C. T.; Gounder, R. Introducing Catalytic Diversity into Single-Site Chabazite Zeolites of Fixed Composition via Synthetic Control of Active Site Proximity. *ACS Catal.* **2017**, *7* (10), 6663−6674.
(28) Kester, P. M.; Crum, J. T.; Li, S.; Schneider, W. F.; Gounder, R. Effects of Brønsted Acid Site Proximity in Chabazite Zeolites on OH Infrared Spectra and Protolytic Propane Cracking Kinetics. *J. Catal.* **2021**, *395*, 210−226.
(29) Di Iorio, J. R.; Li, S.; Jones, C. B.; Nimlos, C. T.; Wang, Y.; Kunkes, E.; Vattipalli, V.; Prasad, S.; Moini, A.; Schneider, W. F.; Gounder, R. Cooperative and Competitive Occlusion of Organic and Inorganic Structure-Directing Agents within Chabazite Zeolites Influences Their Aluminum Arrangement. *J. Am. Chem. Soc.* **2020**, *142* (10), 4807−4819.
(30) Hoffman, A. J.; Bates, J. S.; Di Iorio, J. R.; Nystrom, S. V.; Nimlos, C. T.; Gounder, R.; Hibbitts, D. Rigid Arrangements of Ionic Charge in Zeolite Frameworks Conferred by Specific Aluminum Distributions Preferentially Stabilize Alkanol Dehydration Transition States. *Angew. Chem., Int. Ed.* **2020**, *59* (42), 18686−18694.
(31) Schroeder, C.; Hansen, M. R.; Koller, H. Ultrastabilization of Zeolite Y Transforms Brønsted−Brønsted Acid Pairs into Brønsted−Lewis Acid Pairs. *Angew. Chem., Int. Ed.* **2018**, *57* (43), 14281−14285.
(32) Chen, K.; Abdolrahmani, M.; Horstmeier, S.; Pham, T. N.; Nguyen, V. T.; Zeets, M.; Wang, B.; Crossley, S.; White, J. L. Brønsted−Brønsted Synergies between Framework and Noncrystalline Protons in Zeolite H-ZSM-5. *ACS Catal.* **2019**, *9* (7), 6124−6136.
(33) Timken, H. K. C.; Janes, N.; Turner, G. L.; Lambert, S. L.; Welsh, L. B.; Oldfield, E. Solid-state Oxygen-17 Nuclear Magnetic Resonance Spectroscopic Studies of Zeolites and Related Systems. 2. *J. Am. Chem. Soc.* **1986**, *108* (23), 7236−7241.
(34) Readman, J. E.; Grey, C. P.; Ziliox, M.; Bull, L. M.; Samoson, A. Comparison of the 17O NMR spectra of zeolites LTA and LSX. *Solid State Nucl. Magn. Reson.* **2004**, *26* (3), 153−159.
(35) Peng, L.; Huo, H.; Liu, Y.; Grey, C. P. 17O Magic Angle Spinning NMR Studies of Brønsted Acid Sites in Zeolites HY and HZSM-5. *J. Am. Chem. Soc.* **2007**, *129* (2), 335−346.
(36) Peng, L.; Huo, H.; Gan, Z.; Grey, C. P. 17O MQMAS NMR studies of zeolite HY. *Microporous Mesoporous Mater.* **2008**, *109* (1−3), 156−162.
(37) Huo, H.; Peng, L.; Gan, Z.; Grey, C. P. Solid-State MAS NMR Studies of Brønsted Acid Sites in Zeolite H-Mordenite. *J. Am. Chem. Soc.* **2012**, *134* (23), 9708−9720.
(38) Stebbins, J. F.; Zhao, P.; Lee, S. K.; Cheng, X. Reactive Al-O-Al Sites in a Natural Zeolite; Triple-Quantum Oxygen-17 Nuclear Magnetic Resonance. *Am. Mineral.* **1999**, *84* (10), 1680−1684.
(39) Neuhoff, P. S.; Zhao, P.; Stebbins, J. F. Effect of Extraframework Species on ^{17}O NMR Chemical Shifts in Zeolite A. *Microporous Mesoporous Mater.* **2002**, *55* (3), 239−251.
(40) Perras, F. A.; Wang, Z.; Naik, P.; Slowing, I. I.; Pruski, M. Natural Abundance ^{17}O DNP NMR Provides Precise O−H Distances and Insights into the Brønsted Acidity of Heterogeneous Catalysts. *Angew. Chem., Int. Ed.* **2017**, *56* (31), 9165−9169.
(41) Silaghi, M.-C.; Chizallet, C.; Sauer, J.; Raybaud, P. Dealumination mechanisms of zeolites and extra-framework aluminum confinement. *J. Catal.* **2016**, *339*, 242−255.

https://doi.org/10.1021/jacs.2c05332
J. Am. Chem. Soc. 2022, 144, 16916−16929

(42) Chen, K.; Gan, Z.; Horstmeier, S.; White, J. L. Distribution of Aluminum Species in Zeolite Catalysts: 27Al NMR of Framework, Partially-Coordinated Framework, and Non-Framework Moieties. *J. Am. Chem. Soc.* **2021**, *143* (17), 6669−6680.
(43) Pham, T. N.; Nguyen, V.; Wang, B.; White, J. L.; Crossley, S. Quantifying the Influence of Water on the Mobility of Aluminum Species and Their Effects on Alkane Cracking in Zeolites. *ACS Catal.* **2021**, *11* (12), 6982−6994.
(44) Abdolrahmani, M.; Chen, K.; White, J. L. Assessment, Control, and Impact of Brønsted Acid Site Heterogeneity in Zeolite HZSM-5. *J. Phys. Chem. C* **2018**, *122* (27), 15520−15528.
(45) Heard, C. J.; Grajciar, L.; Rice, C. M.; Pugh, S. M.; Nachtigall, P.; Ashbrook, S. E.; Morris, R. E. Fast Room Temperature Lability of Aluminosilicate Zeolites. *Nat. Commun.* **2019**, *10* (1), 4690.
(46) Pugh, S. M.; Wright, P. A.; Law, D. J.; Thompson, N.; Ashbrook, S. E. Facile, Room-Temperature ^{17}O Enrichment of Zeolite Frameworks Revealed by Solid-State NMR Spectroscopy. *J. Am. Chem. Soc.* **2020**, *142* (2), 900−906.
(47) Lafon, O.; Wang, Q.; Hu, B.; Vasconcelos, F.; Trébosc, J.; Cristol, S.; Deng, F.; Amoureux, J.-P. Indirect Detection via Spin-1/2 Nuclei in Solid State NMR Spectroscopy: Application to the Observation of Proximities between Protons and Quadrupolar Nuclei. *J. Phys. Chem. A* **2009**, *113* (46), 12864−12878.
(48) Brinkmann, A.; Kentgens, A. P. M. Proton-Selective ^{17}O−H Distance Measurements in Fast Magic-Angle-Spinning Solid-State NMR Spectroscopy for the Determination of Hydrogen Bond Lengths. *J. Am. Chem. Soc.* **2006**, *128* (46), 14758−14759.
(49) Gan, Z.; Kwak, H.-T. Enhancing MQMAS Sensitivity Using Signals From Multiple Coherence Transfer Pathways. *J. Magn. Reson.* **2004**, *168* (2), 346−351.
(50) Amoureux, J.-P.; Fernandez, C.; Steuernagel, S. Z-Filtering in MQMAS NMR. *Journal of Magnetic Resonance, Series A* **1996**, *123* (1), 116−118.
(51) Hung, I.; Trébosc, J.; Hoatson, G. L.; Vold, R. L.; Amoureux, J.-P.; Gan, Z. Q-shear Transformation for MQMAS and STMAS NMR spectra. *J. Magn. Reson.* **2009**, *201* (1), 81−86.
(52) Feike, M.; Demco, D. E.; Graf, R.; Gottwald, J.; Hafner, S.; Spiess, H. W. Broadband Multiple-Quantum NMR Spectroscopy. *Journal of Magnetic Resonance, Series A* **1996**, *122* (2), 214−221.
(53) Wang, Q.; Hu, B.; Lafon, O.; Trébosc, J.; Deng, F.; Amoureux, J. P. Double-Quantum Homonuclear NMR Correlation Spectroscopy of Quadrupolar Nuclei Subjected to Magic-Angle Spinning and High Magnetic Field. *J. Magn. Reson.* **2009**, *200* (2), 251−260.
(54) Mali, G.; Fink, G.; Taulelle, F. Double-Quantum Homonuclear Correlation Magic Angle Sample Spinning Nuclear Magnetic Resonance Spectroscopy of Dipolar-Coupled Quadrupolar Nuclei. *J. Chem. Phys.* **2004**, *120* (6), 2835−2845.
(55) Dey, K. K.; Prasad, S.; Ash, J. T.; Deschamps, M.; Grandinetti, P. J. Spectral Editing in Solid-State MAS NMR of Quadrupolar Nuclei using Selective Satellite Inversion. *J. Magn. Reson.* **2007**, *185* (2), 326−330.
(56) Kresse, G.; Furthmüller, J. Efficient Iterative Schemes for ab initio Total-Energy Calculations using a Plane-Wave Basis Set. *Phys. Rev. B* **1996**, *54* (16), 11169.
(57) Perdew, J. P.; Burke, K.; Ernzerhof, M. Generalized Gradient Approximation Made Simple. *Phys. Rev. Lett.* **1996**, *77* (18), 3865.
(58) Kresse, G.; Joubert, D. From Ultrasoft Pseudopotentials to the Projector Augmented-Wave Method. *Phys. Rev. B* **1999**, *59* (3), 1758.
(59) Blöchl, P. E. Projector Augmented-Wave Method. *Phys. Rev. B* **1994**, *50* (24), 17953.
(60) Grimme, S.; Antony, J.; Ehrlich, S.; Krieg, H. A Consistent and Accurate ab initio Parametrization of Density Functional Dispersion Correction (DFT-D) for the 94 Elements H-Pu. *J. Chem. Phys.* **2010**, *132* (15), 154104.
(61) Grimme, S. Supramolecular Binding Thermodynamics by Dispersion-Corrected Density Functional Theory. *Chem.—Eur. J.* **2012**, *18*, 9955−9964.
(62) Li, Y.; Gomes, J.; Sharada, S. M.; Bell, A. T.; Head-Gordon, M. Improved Force-Field Parameters for QM/MM Simulations of the Energies of Adsorption for Molecules in Zeolites and a Free Rotor Correction to the Rigid Rotor Harmonic Oscillator Model for Adsorption Enthalpies. *J. Phys. Chem. C* **2015**, *119* (4), 1840−1850.
(63) Amoureux, J. P.; Bauer, F.; Ernst, H.; Fernandez, C.; Freude, D.; Michel, D.; Pingel, U. T. ^{17}O Multiple-Quantum and ^{1}H MAS NMR Studies of Zeolite ZSM-5. *Chem. Phys. Lett.* **1998**, *285* (1), 10−14.
(64) Bull, L. M.; Bussemer, B.; Anupold, T.; Reinhold, A.; Sauer, J.; Cheetham, A. K.; Dupree, R. A High-Resulotion ^{17}O and ^{29}Si NMR Study of Zeolite Siliceous Ferrierite and ab initio Calculations of NMR Parameters. *J. Am. Chem. Soc.* **2000**, *122*, 4948−4958.
(65) Beck, L. W.; White, J. L.; Haw, J. F. 1H{27Al} Double-Resonance Experiments in Solids: An Unexpected Observation in the 1H MAS Spectrum of Zeolite HZSM-5. *J. Am. Chem. Soc.* **1994**, *116* (21), 9657−9661.
(66) Hunger, M. Multinuclear Solid-State NMR Studies of Acidic and Non-Acidic Hydroxyl Protons in Zeolites. *Solid State Nucl. Magn. Reson.* **1996**, *6* (1), 1−29.
(67) Schroeder, C.; Siozios, V.; Hunger, M.; Hansen, M. R.; Koller, H. Disentangling Brönsted Acid Sites and Hydrogen-Bonded Silanol Groups in High-Silica Zeolite H-ZSM-5. *J. Phys. Chem. C* **2020**, *124* (42), 23380−23386.
(68) Huo, H.; Peng, L.; Grey, C. P. Low Temperature ^{1}H MAS NMR Spectroscopy Studies of Proton Motion in Zeolite HZSM-5. *J. Phys. Chem. C* **2009**, *113* (19), 8211−8219.

NOTE ADDED AFTER ASAP PUBLICATION

After this paper was published August 31, 2022, changes were made to Figure 6 and the accompanying text. The revised version was reposted September 7, 2022.

https://doi.org/10.1021/jacs.2c05332
J. Am. Chem. Soc. 2022, 144, 16916−16929